



Cite this: *Biomater. Sci.*, 2015, 3, 712

Received 21st November 2014,  
Accepted 17th February 2015

DOI: 10.1039/c4bm00402g

www.rsc.org/biomaterialsscience

## Structural and functional changes in high-density lipoprotein induced by chemical modification†

Tatsuya Murakami,\* Haruki Okamoto and Hyungjin Kim

**Reconstituted high-density lipoprotein (rHDL), a natural nanoparticle consisting of apolipoprotein A-I and phospholipids, was modified with a hydrophobic fluorescent dye before (pre-rHDL) and after (post-rHDL) reconstitution. Pre-rHDL particles had a similar size to unmodified rHDL, but post-rHDL particles were significantly larger and their avidity for a HDL receptor was 2.6 times of that shown by pre-rHDL.**

High-density lipoprotein (HDL) mediates reverse cholesterol transport from peripheral tissues to the liver. As HDL can capture drugs administered intravenously and control or influence their biodistribution,<sup>1</sup> it can be used as a natural carrier for targeted drug delivery.<sup>2–4</sup> A nascent form of HDL can be reconstituted from phospholipids and apolipoprotein A-I (apoA-I),<sup>5</sup> and the structure of this nascent form (rHDL) is believed to be a discoidal phospholipid bilayer circumscribed by apoA-I (Fig. 1). Since lysine, arginine, and tyrosine residues can be the sites of chemical modification, multiple chemical engineering strategies have been applied to modify apoA-I for the development of natural, biomaterial-based drug delivery systems.<sup>2,6,7</sup> The pioneering studies by van Berkel's group showed that apoA-I chemical modification enhanced the uptake of intravenously injected lactosylated native HDL<sup>8</sup> and rHDL by rat parenchymal liver cells.<sup>9</sup> Subsequently, folate<sup>10,11</sup> and arginylglycylaspartic acid (RGD peptide)<sup>12</sup> have been used with rHDL for tumor targeting. The targeting ligands have been successfully associated with the apoA-I moiety after mixing with rHDL. However, there is a possibility that hydrophobic ligands such as folate may also become entrapped in the rHDL lipid bilayer, even after repeated dialysis cycles (Fig. 1).

Tetramethylrhodamine isothiocyanate (TRITC) is a primary amine-reactive hydrophobic fluorescent dye, which, if used in rHDL labeling, could be incorporated into the rHDL lipid

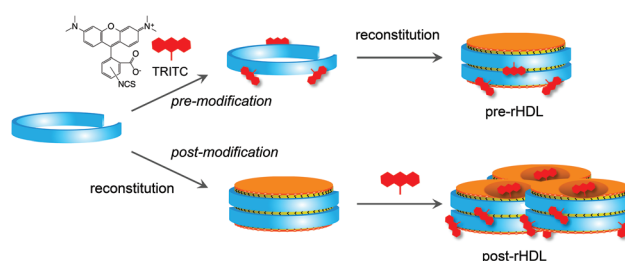


**Fig. 1** Schematic illustration of rHDL modification with TRITC. In the pre-modification scheme, mutated (m)-apoA-I (blue; see the Experimental section in ESI†) was first bound to TRITC (red) and then mixed with phospholipids (orange) for reconstitution. In the post-modification scheme, reconstitution was performed first and then TRITC was conjugated to rHDL, in which case TRITC covalent binding to m-apoA-I can occur simultaneously with its incorporation into the rHDL lipid bilayer due to the hydrophobicity of TRITC. In this study, post-modification yielded enlarged rHDL particles (post-rHDL).

bilayer and could covalently bind to the apoA-I moiety. Although biomedical applications of functionalized rHDL nanoparticles have recently attracted much attention, to our knowledge, there has been no comparative report on the structural and functional effects of apoA-I conjugation with a hydrophobic molecule prior to and after HDL reconstitution (pre- and post-modification, respectively). Here, we used TRITC as a representative hydrophobic molecule to gain fundamental insights into rHDL chemical modifications, and unexpectedly found that the timing of TRITC-apoA-I conjugation significantly influenced the structural and functional properties of rHDL particles.

The reaction conditions for post-modification with fluorescein isothiocyanate<sup>13</sup> were applied for TRITC modification of mutated (m)-apoA-I (in which 43 N-terminal amino acids were deleted) in both pre- and post-modification schemes. It has been reported that m-apoA-I has lipid-binding efficiency and reactivity with lecithin cholesterol acyltransferase (LCAT) similar to those of wild-type apoA-I.<sup>14</sup> Fig. 1 summarizes the modification procedures of rHDL. In pre-modification,

Institute for Integrated Cell-Material Sciences (WPI-iCEMS), Kyoto University, Sakyo-ku, Kyoto 606-8501, Japan. E-mail: murakami@icems.kyoto-u.ac.jp

† Electronic supplementary information (ESI) available. See DOI: 10.1039/c4bm00402g



m-apoA-I was first reacted with TRITC, then unincorporated TRITC was removed by gel chromatography, and the product was freeze-dried and mixed with 1-palmitoyl-2-oleoyl-*sn*-glycero-3-phosphocholine (POPC) for rHDL preparation. In post-modification preparations, freeze-dried m-apoA-I was first mixed with POPC and then reacted with TRITC before purification by gel chromatography and dialysis (molecular weight cut-off, 50 kDa). In these two schemes, rHDL preparation conditions were identical. Fig. S1a† shows sodium dodecyl sulfate-polyacrylamide gel electrophoresis (SDS-PAGE) of TRITC-rHDL complexes (600 ng protein per lane) obtained under various conditions. The fluorescence intensity of TRITC-conjugated m-apoA-I bands was proportional to the amount of added TRITC and was comparable between pre-rHDL and post-rHDL particles obtained using the same TRITC/protein (w/w) ratio. When TRITC was mixed with the protein at a ratio of 0.1 (w/w), calculated based on the number of primary amine groups (20) available in m-apoA-I for the reaction with TRITC, the TRITC/protein molar ratio in pre- and post-rHDL was estimated to be 5.8 at most. However, the band intensity for free TRITC trapped in rHDL lipid bilayers was higher for post-rHDL than for pre-rHDL samples (Fig. S1b†). A small amount of free TRITC detected in pre-rHDL samples may suggest relatively strong physical adsorption of TRITC to m-apoA-I during modification, which could hamper its complete removal. In contrast, higher TRITC incorporation into post-rHDL lipids was inevitable since the hydrophobic TRITC applied to already reconstituted rHDL particles could be retained in the lipid bilayers. Therefore, it was concluded that pre-modification under these conditions had the advantage of producing rHDL particles labeled with TRITC through its specific binding to m-apoA-I.

We next measured the size of rHDL-TRITC conjugates by dynamic light scattering (Fig. 2). Without modification, the mean rHDL diameter under the preparation conditions was  $15.0 \pm 0.4$  nm, which was slightly larger than the 10 nm diameter previously reported for rHDL. The difference may be due to the method used for size analysis (*i.e.*, volume-based dynamic light scattering) and/or the reconstitution procedure (application of urea for m-apoA-I solubilization; see the Experimental section in ESI†). In the pre-rHDL preparations, the mean diameter barely changed, regardless of the protein/TRITC molar ratio; however, a significant increase in diameter (more than two- or three-fold) was observed for post-rHDL particles after conjugation with TRITC (Table 1).

Very large nanoparticles ( $\geq 100$  nm in diameter) could represent not only rHDL aggregates but also POPC liposomes and/or cholate/POPC micelles, possibly formed by lipid impurities contaminating rHDL prepared by the cholate dialysis method. To check this possibility, we performed gel chromatography analysis, which clearly excluded the presence of POPC liposomes, because their retention time (11.3 min for 116 nm liposomes) was significantly shorter than that of post-rHDL particles (13.3 min) (Fig. S2†).

We also examined cholate/POPC micelles prepared according to the cholate dialysis method without protein addition

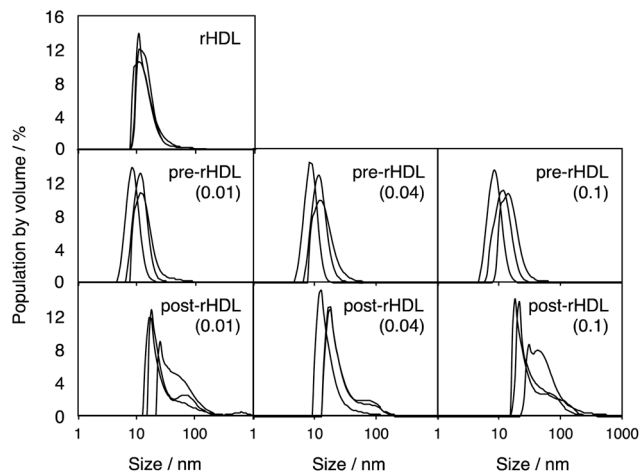


**Fig. 2** Size distribution of pre-rHDL and post-rHDL particles. Pre-rHDL (middle panels) and post-rHDL (bottom panels) particles were prepared at the TRITC/protein (w/w) ratios of 0.01, 0.04, and 0.1, as indicated in each panel. Unconjugated rHDL (designated as rHDL) is shown as a reference (upper panel). Size distribution and mean size of pre-rHDL particles appeared unchanged from those of rHDL. However, for post-rHDL samples, size distribution broadening towards larger particles was clearly observed. The data for each rHDL sample represent the mean of three independent preparations.

**Table 1** Mean size and yield of pre-rHDL and post-rHDL particles

	TRITC/protein ratio	Mean size <sup>a</sup> (nm)	Yield <sup>a</sup> (% w/w protein)
rHDL	—	$15 \pm 0.4$	$59 \pm 5.4$
Pre-rHDL	0.01	$11 \pm 2.9$	$57 \pm 3.6$
	0.04	$12 \pm 3.1$	$64 \pm 5.0$
	0.1	$12 \pm 3.7$	$60 \pm 4.7$
Post-rHDL	0.01	$46 \pm 11$	$56 \pm 1.6$
	0.04	$27 \pm 4.5$	$64 \pm 2.4$
	0.1	$52 \pm 8.6$	$55 \pm 3.6$

<sup>a</sup> Average  $\pm$  standard deviation of three preparations.

(see the experimental section in ESI†). The micelles had a mean size of  $\sim 28$  nm, which did not change even after mixing with TRITC (Fig. S3†), suggesting that the enlarged nanoparticles in post-rHDL samples were not cholate/POPC micelles. Taken together, these results indicate that the fraction of enlarged post-rHDL particles is represented by rHDL aggregates.

Cellular dynamics of rHDL-TRITC conjugates were investigated in Chinese hamster ovary (CHO) cells overexpressing the HDL receptor SR-BI.<sup>15</sup> CHO-SR-BI cells were treated with pre-rHDL and post-rHDL particles prepared at the TRITC/protein ratio of 0.1/1 in serum-containing medium for 1 h. Both pre-rHDL and post-rHDL particles demonstrated diffuse cellular distribution and minimal colocalization with late endosomes/lysosomes (Fig. 3), which is consistent with previous observations showing that after endocytosis under normal conditions, HDL is recycled through the endosome recycling



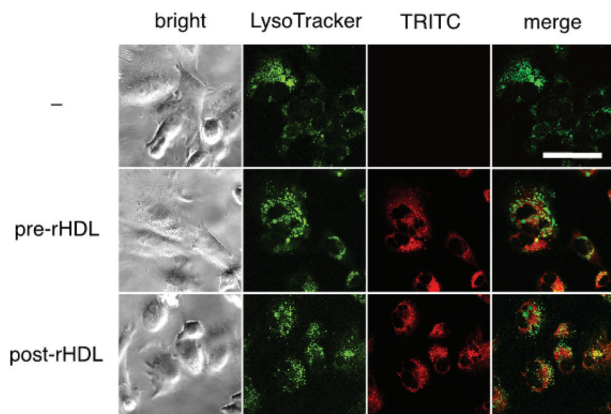


**Fig. 3** Confocal images of CHO-SR-BI cells treated with pre-rHDL or post-rHDL nanoparticles. Cells were incubated with pre-rHDL or post-rHDL samples ( $10 \mu\text{g protein mL}^{-1}$  at a TRITC/protein ratio of 0.1) for 1 h at  $37^\circ\text{C}$  and stained with LysoTracker (green) to reveal late endosomes/lysosomes. Subcellular localization of rHDL particles was analyzed by TRITC fluorescence (red), which showed little colocalization with late endosomes/lysosomes for both rHDL samples despite a significant difference in particle size (Table 1). Scale bar,  $50 \mu\text{m}$ .

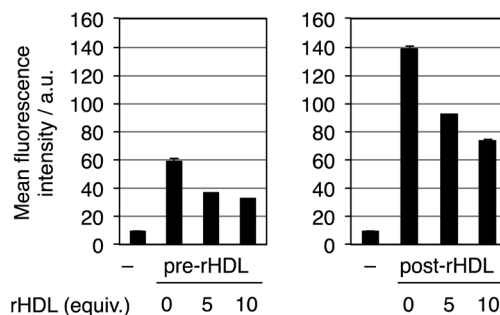


**Fig. 4** FACS analysis of pre-rHDL (left panel) and post-rHDL (right panel) binding to CHO-SR-BI cells. Cells were incubated with pre-rHDL ( $15 \mu\text{g protein mL}^{-1}$ ) or post-rHDL ( $10 \mu\text{g protein mL}^{-1}$ ) particles (TRITC/protein ratio, 0.1/1) in the presence or absence of non-labeled rHDL (rHDL) at  $37^\circ\text{C}$  for 1 h. The concentration of pre-rHDL and post-rHDL particles was adjusted to TRITC equivalent, and that of non-labeled rHDL was adjusted to protein equivalent. The total binding efficiency of post-rHDL particles was 2.6 times that of pre-rHDL particles, while SR-BI-dependency of their binding was similar. The analysis was performed in triplicate.

compartment<sup>16</sup> and is transported to the Golgi apparatus in SR-BI-overexpressing cells.<sup>17</sup> Importantly, these results also indicate that the size increase did not seem to have a significant impact on cellular dynamics of post-rHDL-TRITC conjugates because they did not follow the tendency of large ( $\sim 100 \text{ nm}$ ) nanoparticles such as liposomes to accumulate in endolysosomes. However, post-rHDL particles showed a significant presence in the mitochondria (Fig. S4†). Given that TRITC alone tended to accumulate in the mitochondria (Fig. S4†), this may be due to a significant presence of free TRITC in post-rHDL lipid bilayers (Fig. S1†).

The effects of pre- and post-reconstitution modifications on rHDL binding ability to the SR-BI receptor were examined in CHO-SR-BI cells treated with pre-rHDL ( $15 \mu\text{g protein mL}^{-1}$ ) or post-rHDL ( $10 \mu\text{g protein mL}^{-1}$ ) particles (TRITC/protein ratio, 0.1) adjusted by TRITC content. To our knowledge, the binding of rHDL, including m-apoA-I, to the SR-BI receptor has not been reported yet; however, a similarly mutated rHDL, in which 59 N-terminal amino acids of apoA-I were deleted, has demonstrated a slightly higher avidity for SR-BI compared to the wild-type rHDL and native HDL.<sup>18</sup> Fluorescence-activated cell sorter (FACS) analysis revealed that the mean fluorescence intensities were significantly different between the two samples: 60 versus 140 for pre-rHDL and post-rHDL samples, respectively (Fig. 4). In competition experiments using five- or ten-fold excess of non-labeled rHDL, the binding of pre-rHDL and post-rHDL particles was inhibited to a similar extent (45% or 53% and 36% or 50%, respectively). Given the significant diffusion of free TRITC in the lipid bilayers of post-rHDL particles, these results can be explained by receptor-independent internalization of non-covalently bound TRITC, which produced an additional fluorescence response. However, competition assays revealed a similar degree of fluorescence

inhibition (Fig. 4), ruling out non-specific effects. It is also unlikely that the TRITC modification contributed to the increased hydrophobicity of post-rHDL, because the amount of m-apoA-I-bound TRITC in these samples was similar (Fig. S1c†). Finally, the alterations in the surface structure due to size variations can also be excluded because of similarity in zeta potential for pre-rHDL ( $-27 \pm 2.3 \text{ mV}$ ) and post-rHDL ( $-26 \pm 1.3 \text{ mV}$ ) particles.

We attribute the difference in cell fluorescence to the larger size of post-rHDL particles ( $52 \pm 8.6 \text{ nm}$  versus  $12 \pm 3.7 \text{ nm}$  for pre-rHDL). It has been shown that the concentration of the SR-BI ligand apoA-I per particle is increased proportionally to the particle size,<sup>19</sup> suggesting that large post-rHDL particles have higher avidity to the HDL receptor. TRITC-embedded cholate/POPC micelles, the lipid impurities in post-rHDL samples (Fig. S5†), were able to bind SR-BI under the same conditions with efficiency comparable to that of pre-rHDL particles, but there was no competition for binding with rHDL (Fig. S6†). In addition, given the physiological function of SR-BI,<sup>20</sup> the increased avidity of post-rHDL to SR-BI may be attributed to the higher content of free TRITC embedded in the post-rHDL lipid bilayer (Fig. S1b†); however, quantitative analysis of the confocal images shown in Fig. S4† suggests that its contribution was insignificant (Fig. S7†). Therefore, our results suggest that the higher avidity of post-rHDL particles to the receptor is mainly the result of their increased size. The enhanced binding of chemically modified rHDL to the SR-BI receptor can be used in drug delivery research for developing a novel strategy to control rHDL biodistribution.

Finally, we examined the dynamics of rHDL enlargement by post-reconstitution TRITC modification. Decreasing the reaction time from 24 h to 4 h resulted in smaller particle sizes and lower protein labeling efficiency, whereas TRITC embedded in the lipid bilayer was unchanged (Fig. S8†).



Surprisingly, when TRITC freshly prepared in dimethylsulfoxide (DMSO; see the experimental section in ESI†) was used, there was no particle enlargement, even after 24 h reaction. On the other hand, the protein labeling efficiency was significantly higher than that of the samples prepared with TRITC stored at  $-30\text{ }^{\circ}\text{C}$ , whereas lipid embedding was similar for both types of TRITC (Fig. S8†). These findings could be attributed to the decreased reactivity of the TRITC isothiocyanate group.

In summary, we compared the effects of chemical conjugation with TRITC, a hydrophobic fluorescent dye, on the structure and function of rHDL particles assembled before and after TRITC modification. Compared with pre-rHDL particles, post-rHDL particles showed a significantly larger mean size, and incorporated more TRITC in the lipid bilayer. In HDL receptor-overexpressing cells, the two types of rHDL-TRITC conjugates showed similar intracellular distribution; however, post-rHDL particles had a significantly higher binding efficiency, most probably due to their increased size. This study identified a previously unknown phenomenon that should be considered in rHDL chemical modifications and could be applied to the development of novel strategies in the design of rHDL-based drug delivery systems.

## Acknowledgements

This work was supported by the World Premier International Research Center Initiative (WPI), MEXT, Japan, and by Grant-in-Aid for Challenging Exploratory Research, MEXT, Japan (T.M.).

## Notes and references

- 1 A. Barel, G. Jori, A. Perin, P. Romandini, A. Pagnan and S. Biffanti, *Cancer Lett.*, 1986, **32**, 145–150.
- 2 P. C. N. Rensen, R. L. A. de Vruhe, J. Kuiper, M. K. Bijsterbosch, E. A. L. Biessen and T. J. C. van Berkel, *Adv. Drug Delivery Rev.*, 2001, **47**, 251–276.
- 3 R. O. Ryan, *Expert Opin. Drug Delivery*, 2008, **5**, 343–351.
- 4 K. M. McMahon and C. S. Thaxton, *Expert Opin. Drug Delivery*, 2014, **11**, 231–247.
- 5 A. Jonas, in *Methods Enzymol.*, ed. J. P. Segrest and J. J. Albers, Academic Press, Inc., Orlando, USA, 1986, vol. 128, pp. 553–582.
- 6 K. K. Ng, J. F. Lovell and G. Zheng, *Acc. Chem. Res.*, 2011, **44**, 1105–1113.
- 7 T. Murakami, *Biotechnol. J.*, 2012, **7**, 762–767.
- 8 M. K. Bijsterbosch and T. J. C. van Berkel, *Mol. Pharmacol.*, 1992, **41**, 404–411.
- 9 M. K. Bijsterbosch, H. van de Bilt and T. J. C. van Berkel, *Biochem. Pharmacol.*, 1996, **52**, 113–121.
- 10 I. R. Corbin, J. Chen, W. Cao, H. Li, S. Lund-Katz and G. Zheng, *J. Biomed. Nanotechnol.*, 2007, **3**, 367–376.
- 11 T. Murakami, W. Wijagkanalan, M. Hashida and K. Tsuchida, *Nanomedicine*, 2010, **5**, 867–879.
- 12 W. Chen, P. A. Jarzyna, G. A. F. van Tilborg, V. A. Nguyen, D. P. Cormode, A. Klink, A. W. Griffioen, G. J. Randolph, E. A. Fisher, W. J. M. Mulder and Z. A. Fayad, *FASEB J.*, 2010, **24**, 1689–1699.
- 13 K. Takata, S. Horiuchi, A. Torab, M. A. Rahim and Y. Morino, *J. Lipid Res.*, 1988, **29**, 1117–1126.
- 14 D. P. Rogers, C. G. Brouillette, J. A. Engler, S. W. Tendian, L. Roberts, V. K. Mishra, G. M. Anantharamaiah, S. Lund-Katz, M. C. Phillips and M. J. Ray, *Biochemistry*, 1997, **36**, 288–300.
- 15 M. Fukasawa, H. Adachi, K. Hirota, M. Tsujimoto, H. Arai and K. Inoue, *Exp. Cell Res.*, 1996, **222**, 246–250.
- 16 C. Röhrlich and H. Stangl, *Biochim. Biophys. Acta*, 2013, **1831**, 1626–1633.
- 17 S. Rhode, A. Breuer, J. Hesse, M. Sonnleitner, T. A. Pagler, M. Doring, G. J. Schütz and H. Stangl, *Cell Biochem. Biophys.*, 2004, **41**, 343–356.
- 18 K. N. Liadaki, T. Liu, S. Xu, B. Y. Ishida, P. N. Duchateaux, J. P. Krieger, J. Kane, M. Krieger and V. I. Zannis, *J. Biol. Chem.*, 2000, **275**, 21262–21271.
- 19 J. B. Massey and H. J. Pownall, *Biochim. Biophys. Acta*, 2008, **1781**, 245–253.
- 20 S. Acton, A. Rigotti, K. T. Landschulz, S. Xu, H. H. Hobbs and M. Krieger, *Science*, 1996, **271**, 518–520.

